The clathrin heavy chain isoform CHC22 functions in a novel endosomal sorting step

Christopher Esk,[1,2,3,4] Chih-Ying Chen,[1,2,3,4] Ludger Johannes,[5,6] and Frances M. Brodsky[1,2,3,4]

[1]Department of Bioengineering and Therapeutic Sciences, [2]Department of Pharmaceutical Chemistry, [3]Department of Microbiology and Immunology, and [4]The G.W. Hooper Foundation, University of California, San Francisco, San Francisco, CA 94143
[5]Institut Curie, Centre de Recherche, Traffic, Signaling and Delivery Laboratory, 75248 Paris Cedex 05, France
[6]UMR144 Centre National de la Recherche Scientifique, France

Clathrin heavy chain 22 (CHC22) is an isoform of the well-characterized CHC17 clathrin heavy chain, a coat component of vesicles that mediate endocytosis and organelle biogenesis. CHC22 has a distinct role from CHC17 in trafficking glucose transporter 4 (GLUT4) in skeletal muscle and fat, though its transfection into HEK293 cells suggests functional redundancy. Here, we show that CHC22 is eightfold less abundant than CHC17 in muscle, other cell types have variably lower amounts of CHC22, and endogenous CHC22 and CHC17 function independently in nonmuscle and muscle cells. CHC22 was required for retrograde trafficking of certain cargo molecules from endosomes to the trans-Golgi network (TGN), defining a novel endosomal-sorting step distinguishable from that mediated by CHC17 and retromer. In muscle cells, depletion of syntaxin 10 as well as CHC22 affected GLUT4 targeting, establishing retrograde endosome–TGN transport as critical for GLUT4 trafficking. Like CHC22, syntaxin 10 is not expressed in mice but is present in humans and other vertebrates, implicating two species-restricted endosomal traffic proteins in GLUT4 transport.

Introduction

Clathrin heavy chain 17 (CHC17) is well characterized as a coat protein required for vesicle formation at the plasma membrane, the TGN, and endosomes (Brodsky et al., 2001). Most vertebrates have a second clathrin heavy chain isoform (CHC22), with each isoform named for the encoding human chromosome. We recently identified a role for CHC22 in trafficking the glucose transporter 4 (GLUT4) in skeletal muscle and fat (Vassilopoulos et al., 2009), which is independent from that of CHC17. In apparent contrast, a recent study of transfected cells suggested functional redundancy of the CHCs (Hood and Royle, 2009). The study reported here localizes the distinct function of endogenous CHC22 relative to the known cellular functions of CHC17 and thereby defines the specialized contribution of CHC22 to membrane traffic pathways.

CHC17 and CHC22 have 85% sequence identity; however, key residue differences have been conserved during evolution. These are predominantly found in regions that bind clathrin adaptors and the regulatory clathrin light chains (CLCs) in CHC17 (Wakeham et al., 2005). CHC17 interactions with adaptor proteins are required for cargo capture and cellular localization of CHC17 lattice formation on membranes and vesicles (Brodsky et al., 2001). These processes involve adaptor protein (AP) complex AP1 and Golgi-localized, gamma ear–containing, ARF-binding proteins (GGAs) 1–3 at the TGN, AP1, AP3, and probably GGAs at endosomes, and AP2 at the plasma membrane (Benmerah and Lamaze, 2007; Ungewickell and Hinrichsen, 2007). CHC22 associates with AP1 and AP3 adaptors but not the endocytic AP2 complex (Liu et al., 2001; Vassilopoulos et al., 2009). Consequently, skeletal muscle cells depleted of CHC22 show normal endocytosis (Vassilopoulos et al., 2009). Both CHCs form trimers but do not cotrimerize or coassemble and CHC22 does not bind CLCs, which influence CHC17 assembly and interaction with the actin cytoskeleton (Chen and Brodsky, 2005). In place of CLCs, CHC22 can bind sorting nexin 5 (SNX5), a participant in macropinocytosis and retromer-mediated retrograde transport (Towler et al., 2004; Kerr et al., 2006; Wassmer et al.,

Correspondence to Frances M. Brodsky: Frances.Brodsky@ucsf.edu

Abbreviations used in this paper: AP, adaptor protein; CHC, clathrin heavy chain; CI-MPR, cation-independent mannose-6-phosphate receptor; CLC, clathrin light chain; GGA, Golgi-localized, gamma ear–containing ARF-binding protein; GLUT4, glucose transporter 4; GSC, GLUT4 storage compartment; KDP, knockdown proof; SNX, sorting nexin; STX, syntaxin; STxB, Shiga toxin B-subunit.

The Rockefeller University Press $30.00
J. Cell Biol. Vol. 188 No. 1 131–141
www.jcb.org/cgi/doi/10.1083/jcb.200908057

2007, 2009; Lim et al., 2008). Despite the described differences between CHCs, a recent study demonstrated that transfected CHC22 could rescue CHC17 function after CHC17 depletion by siRNA (Hood and Royle, 2009). This raised issues of CHC competition and redundancy and whether a dominant pathway for endogenous CHC22 function can be defined.

GLUT4 is expressed in muscle and adipocytes, where it is concentrated in the insulin-regulated GLUT4 storage compartment (GSC) and colocalizes with CHC22, which is involved in GSC formation (Vassilopoulos et al., 2009). Traffic to and from the GSC, derived from both the endocytic and secretory pathways, involves ubiquitous membrane traffic mediators including SNAREs, AP1, GGAs, and CHC17 as well as some proteins with tissue-restricted expression (Hou and Pessin, 2007; Huang and Czech, 2007). GLUT4 itself shares ubiquitous trafficking pathways with endocytic and retrograde cargo in the endosomal system such as transferrin receptor and the cation-independent mannose-6-phosphate receptor (CI-MPR; Karylowski et al., 2004; Huang and Czech, 2007). Hence, the CHC22 pathway contributing to GSC formation may be restricted to GSC-bound cargo but could also represent a ubiquitous trafficking pathway. Mapping the precise trafficking step where CHC22 operates and establishing the extent of its intracellular role characterizes a pathway that contributes to GSC formation, a process that has considerable relevance to type 2 diabetes, where GSC function is defective (Garvey et al., 1998; Maianu et al., 2001).

A notable feature of CHC22 is its absence from the *Mus* (murine) genome (Wakeham et al., 2005). Indeed, expression of human CHC22 in transgenic mice leads to a GLUT4 trafficking defect, resulting in features of diabetes (Vassilopoulos et al., 2009). In addition to implicating CHC22 in GLUT4 trafficking, the transgenic mouse phenotype suggests the possibility that other species-restricted proteins involved in membrane traffic might function in concert with CHC22. Such trafficking proteins that are present in humans but not in mice include TBC1D3, a GGA-binding mediator of macropinocytosis (Frittoli et al., 2008; Wainszelbaum et al., 2008) and syntaxin 10 (STX10), a SNARE involved in retrograde endosomal sorting (Tang et al., 1998; Ganley et al., 2008). The studies reported here demonstrate that STX10 plays a role in GSC formation, establishing a connection between STX10 and CHC22 function and implicating endosomal traffic in GSC formation. Through analysis of the role of CHC22 in sorting additional cargo in HeLa cells, we also establish that the two CHC isoforms indeed mediate distinct intracellular membrane traffic pathways and that CHC22 function defines a novel step in endosomal sorting in nonmuscle cells. Finally, by demonstrating a comparable function for CHC22 in skeletal muscle cells, we define a role for this pathway in GLUT4 trafficking.

Results

CHC22 function segregates from CHC17 function and its localization is restricted to endosomes

We established both absolute and relative levels of endogenous expression of the two CHCs in different cell types, in order to understand the apparently discrepant results from studies describing their functional differentiation or compensation (Hood and Royle, 2009; Vassilopoulos et al., 2009). Levels of CHC22 relative to total protein varied between nine cell lines analyzed, derived from different tissues (Fig. 1 A). Myoblast cultures and HeLa cells had the highest expression. Cell lines derived from other human tissues all expressed some CHC22, but considerably less, with the lowest expression in the liver cell line HepG2 and the natural killer cell line NKL. This is consistent with predicted expression based on mRNA levels in different tissues (Kedra et al., 1996; Sirotkin et al., 1996). The murine skeletal muscle cell line C2C12 had no CHC22 protein, as expected from the murine CHC22 pseudogene. The levels of CHC17 were far less variable between cell lines, indicating that the ratios of CHC22 to CHC17 vary between tissues. To determine these ratios from absolute protein levels of each CHC, the antibodies used for immunoblotting were calibrated against known amounts of recombinant protein fragments of each CHC. Dilutions of cell lysates were correlated with these standards based on immunoblotting signals (Fig. 1 B). These experiments revealed that the ratios of CHC22 to CHC17 are ∼1:8 for LHCNM2 and 1:12 in HeLa. Thus, under endogenous conditions, there is 8- to 12-fold more CHC17 in cells than CHC22, even in cells that have the highest amount of CHC22.

To further study the functional relationship between CHCs at normal levels of expression, we used siRNA to individually down-regulate both CHCs in HeLa cells (Fig. 1 C). In nontreated cells (not depicted) and cells treated with control siRNA, immunofluorescence detection of CHC22 revealed a punctate staining pattern with a more uniform intracellular distribution than CHC17, lacking the strong perinuclear crescent typical of CHC17 labeling in the TGN. Minor colocalization between CHC22 and CHC17 was confined to peripheral compartments (Fig. 1 D; Fig. S1 A). In cells depleted of CHC17, CHC22 staining appeared marginally brighter in the perinuclear region (Fig. 1 E; Fig. S1 B) and there was slightly more CHC22 colocalized with AP1 (Fig. S1 E) compared with control-treated cells (Fig. S1 D). This change in distribution may reflect increased membrane recruitment of CHC22 in the absence of CHC17, accounting for the modest increase in CHC22 protein levels detected by immunoblotting after CHC17 depletion (Fig. 1 C). In contrast, CHC17 distribution and levels (Fig. 1 F; Fig. S1 C) were unaffected by depletion of CHC22, as were CLC protein levels (Fig. 1 C), corroborating no detectable biochemical interaction between CHC22 and CLCs or CHC17 (Liu et al., 2001). By comparison, depletion of CHC17 profoundly reduced CLC levels. Together, these depletion studies indicate that under endogenous conditions, CHC22 is outcompeted for localization to the TGN by CHC17.

Consistent with CHC22 showing no coimmunoprecipitation with the endocytic adaptor AP2 (Liu et al., 2001; Vassilopoulos et al., 2009), CHC22 was not observed at the plasma membrane, even in the absence of CHC17, and depletion of CHC22 had no effect on endocytosis of transferrin by HeLa cells (Fig. 1, D–F). These results correlated with no observed effect on EGF uptake after CHC22 depletion from LHCNM2 myoblasts (Vassilopoulos et al., 2009). In contrast, CHC17 depletion strongly inhibited transferrin endocytosis (Fig. 1, D–F), as described previously

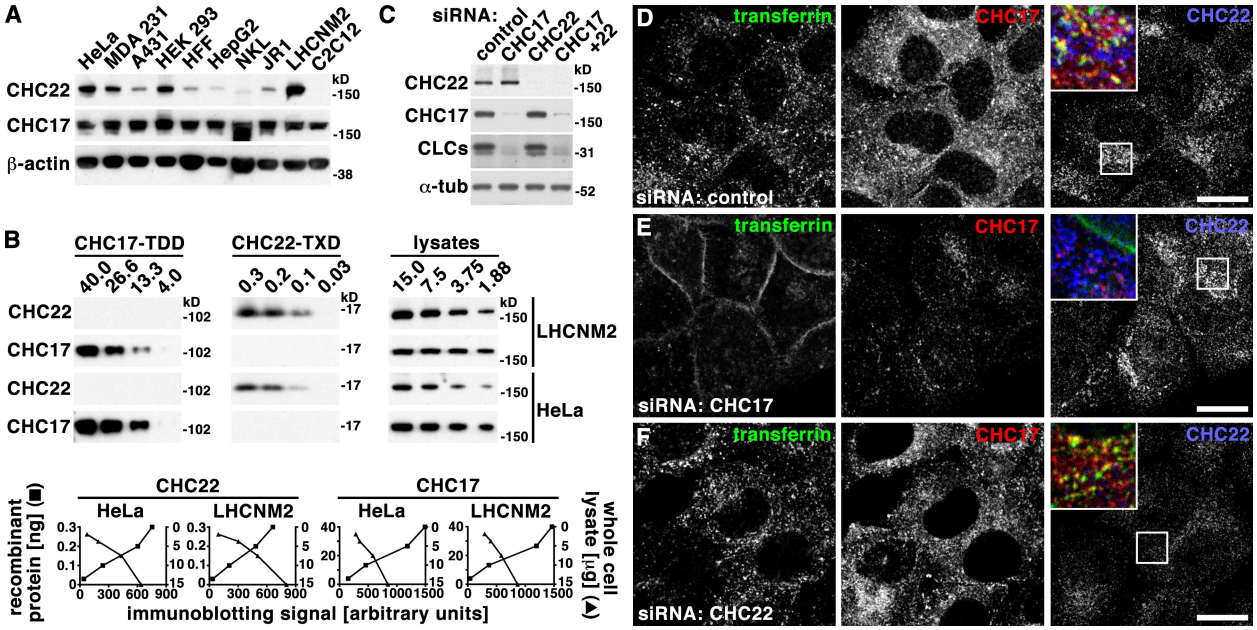

Figure 1. **CHC22 is present at variable levels in most cell types and does not participate in endocytosis.** (A) Detergent lysates of 10 tissue culture cell lines (equalized for protein content) were separated by SDS-PAGE and immunoblotted with antibodies against proteins indicated at the left. Tissue sources for the cell lines were cervical epithelium (HeLa), mammary gland epithelium (MDA 231), epidermal epithelium (A431), kidney epithelium (HEK 293), foreskin fibroblast (HFF), hepatocellular carcinoma (HepG2), natural killer lymphocyte (NKL), rhabdomyosarcoma (JR1), and skeletal muscle (LHCNM2 and C2C12), with all derived from human samples except C2C12 (mouse). (B) Indicated amounts of recombinant protein fragments (in ng) of CHC17 (amino acids 1–1074, CHC17-TDD) or CHC22 (amino acids 1521–1640, CHC22-TXD) and of detergent lysates (in μg) of HeLa or LHCNM2 cells (designated at the far right) were separated by SDS-PAGE and analyzed sequentially on the same immunoblot, after stripping in between, with antibodies against the CHC for the entire row indicated at the left. Below, each plot shows the intensity of the immunoblotting signal (x-axis) versus the amount of recombinant protein (left y-axis, solid squares) or detergent lysate (right y-axis, solid triangles) analyzed. CHC amount in cell lysates was determined by intersection with the immunoblotting signals from the recombinant fragments used for antibody calibration, adjusting for fragment length. Measured ratios for CHC22 compared with CHC17 were 1:8 for LHCNM2 and 1:12 for HeLa. (C) Detergent lysates of HeLa cells treated with siRNA to deplete CHCs indicated at the top or with control siRNA were separated by SDS-PAGE and immunoblotted with antibodies against proteins indicated at the left. α-Tubulin (α-tub) serves as a loading control. (D–F) HeLa cells treated with control siRNA (D) or siRNA to deplete cells of CHC17 (E) and CHC22 (F) were incubated with fluorescent transferrin (green in merged insets) and internalization was allowed for 10 min. Cells were then fixed and processed for double immunofluorescence using antibodies against CHC17 (red in merged insets) or CHC22 (blue in merged insets) as indicated. Bars, 20 μm.

(Hinrichsen et al., 2003; Motley et al., 2003). However, it was recently demonstrated that supertransfected CHC22 rescued endocytosis defects caused by CHC17 depletion (Hood and Royle, 2009). The GFP-CHC22 construct used in that study was driven by a CMV promotor, resulting in high expression. The compensation by CHC22 in the absence of CHC17 raised the question of whether higher-than-natural levels of CHC22 could compete for endogenous CHC17. To address this, we reproduced the CMV promoter-driven GFP-CHC22 construct, making sure it was full length and not missing the apparently labile exon 9 (Hood and Royle, 2009). After transient transfection of HeLa cells, colocalization between CHC17 and CHC22 was assessed by antibody detection of both endogenous and artificially introduced protein, comparing nontransfected (Fig. 2 A) with transfected cells (Fig. 2 B) in the same culture. High levels of GFP-CHC22 caused increased (three- to fourfold) colocalization of the two CHCs (Fig. 2 C). Thus, when CHC22 is expressed in excess, it can localize to the same cellular regions as CHC17. It is notable that neither the location nor intensity of CHC17 staining was altered by the presence of GFP-CHC22, suggesting that the introduced protein could not compete with endogenous CHC17 when present. Furthermore, CHC22 does not compensate for CHC17 function if absent and CHC22 is expressed at its relatively low endogenous levels (Fig. 1, D–F), so the apparently redundant function of the two CHCs occurs only if CHC17 is absent and CHC22 is highly overexpressed. Similar considerations apply to CHC22 substitution for CHC17 function in mitotic spindle dynamics, as we did not detect CHC22 by antibody staining on spindles in either control cells or cells depleted of CHC17 (Fig. S1, F and G).

Lack of localization of CHC22 with TGN (perinuclear AP1, TGN46; Fig. S1 D, Fig. S2, A and B) and plasma membrane markers (AP2; Fig. S2 C) prompted us to study CHC22 in the endosomal system where subpopulations of AP1 and AP3 are present (Dell'Angelica et al., 1997; Meyer et al., 2000). CHC22 did not localize with early endosomal antigen EEA1 or recycling endosomal Rab11 (Fig. 3, A and B; Fig. S2, G and H), but partially overlapped with the late endosome marker Rab9 (Fig. 3 C; quantified in Fig. S2, G and H). Lesser overlap was seen with AP3 (Fig. S2 E) and sorting nexins SNX5 (Fig. S2 D) and SNX1 (Fig. S2 F), which are present in endosomal sorting domains. Treatment of cells with Brefeldin A disrupted the characteristic TGN localization of CHC17 (Wong and Brodsky, 1992) but did not affect overall CHC22 distribution or CHC17 distribution in endosomal regions (Fig. S3). Hence, endogenous CHC22 is confined to endosomes. We therefore tested a role for CHC22 in distinct endosomal sorting pathways defined by model cargo molecules.

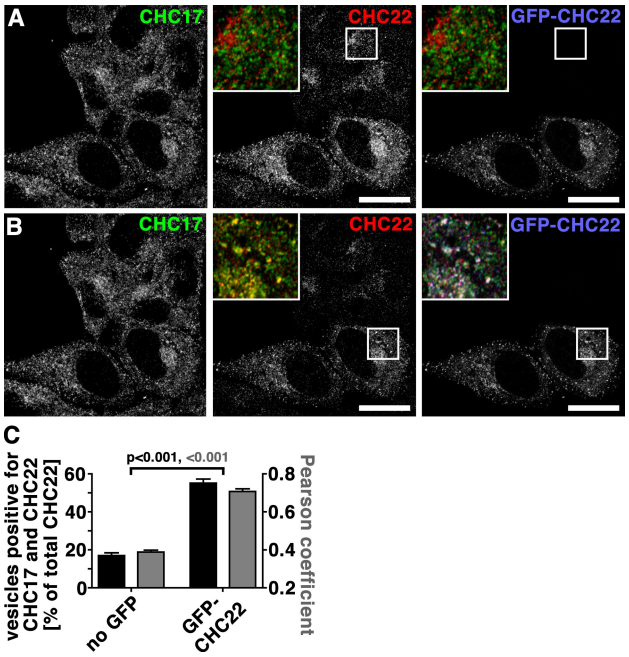

Figure 2. **Overexpression of CHC22 increases its colocalization with CHC17.** (A and B) HeLa cells transfected with GFP-tagged CHC22 (GFP-CHC22, blue in merged insets) were processed for immunofluorescence and labeled for CHC17 (green in merged insets) and CHC22 (red in merged insets) as indicated. CHC22 label was imaged with microscope settings optimal for nontransfected cells (A) or transfected cells (B). Merged images of the boxed area consisting of CHC17 and CHC22 antibody labeling in the middle panels and all three signals in the right images are presented as an inset. Bars, 20 µm. (C) Vesicles containing both CHC17 and CHC22 or CHC22 only were automatically counted in nontransfected (no GFP) or transfected cells (GFP-CHC22). The percentage of vesicles containing both CHCs relative to all CHC22-positive vesicles is plotted (black bars) against the left y-axis for individual cells (n = 12 each of transfected or nontransfected cells from two independent experiments). Average percentages are shown ± SEM. Pearson's coefficients of colocalization were determined for cells from the same experiment and plotted ± SEM (gray bars) against the right y-axis (n = 12 each of transfected or nontransfected cells from two independent experiments). P-values for respective evaluation are indicated according to color code.

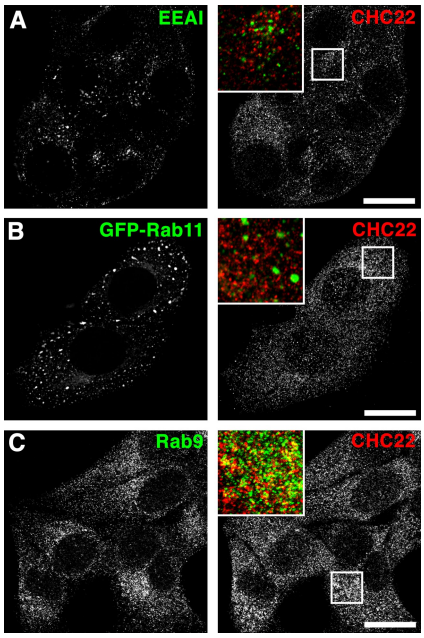

Figure 3. **CHC22 partially colocalizes with the endosomal marker Rab9.** HeLa cells were grown on coverslips, processed for immunofluorescence, and labeled for CHC22 (red in merged insets). Simultaneous labeling was performed (green in merged insets) using mouse monoclonal antibodies against (A) EEA1 and (C) Rab9. (B) Rab11 was visualized as a GFP fusion protein after transient transfection of HeLa cells. Bars, 20 µm.

CHC17 and CHC22 act independently in endosomal sorting

Previous studies using dominant-negative constructs of the two CHCs representing the C-terminal third (Hub) of each protein suggested that they are both involved in CI-MPR localization. The CHC22 Hub caused dispersion of the CI-MPR from its normal perinuclear focus (Liu et al., 2001) and the CHC17 Hub induced a tighter perinuclear distribution than normal (Bennett et al., 2001). In the present study, similar effects were observed after treatment of HeLa cells with siRNAs targeting each CHC (Fig. 4). In comparison to the loose perinuclear concentration of CI-MPR in late endosomes in control cells (Fig. 4, A and C; Fig. 5, A and C), CHC17 depletion induced a slightly tighter perinuclear concentration, as reported previously (Hinrichsen et al., 2003; Fig. 4 D, Fig. 5 D). In contrast, after CHC22 depletion, CI-MPR was quantitatively more dispersed throughout the cytosol in small vesicular structures (Fig. 4, B, E and F; Fig. 5, B and E), as assessed by measuring levels of CI-MPR peripheral to the Golgi region (see illustrative Fig. S4). Expression of an siRNA-resistant (knock-down proof [KDP]), FLAG-tagged CHC22 construct completely reversed the effects induced by siRNA targeting of CHC22 without affecting control-treated or CHC17-depleted cells (Fig. 4, C–F), further indicating that the two CHCs act at separate stages of CI-MPR transport. CHC-depleted cells were tested for secretion of the lysosomal hydrolase hexosaminidase (Fig. 4 G), a hallmark of mis-sorting of CI-MPR at the TGN (Riederer et al., 1994). CHC17 and CHC22 loss resulted in a respective 70% or 22% increase of secreted hexosaminidase, with the considerably stronger effect of CHC17 corroborating its role in sorting CI-MPR at the TGN. Simultaneous depletion of CHCs appeared to increase hexosaminidase secretion in an additive fashion, though not statistically significant compared with CHC17 depletion alone, supporting roles for each CHC at distinct steps of CI-MPR traffic.

The punctate distribution of CI-MPR in CHC22-depleted cells suggested that it might be trapped in some stage of the endosomal pathway. Furthermore, CI-MPR did not colocalize with CHC17 in CHC22-depleted cells, indicating that CI-MPR was not present in the TGN upon loss of CHC22 (Fig. 5 B). CI-MPR sorting in the endosomal pathway requires CHC17 and retromer for retrograde exit from EEA1-positive endosomes (Arighi et al., 2004; Saint-Pol et al., 2004; Seaman, 2004). Consequently, CI-MPR showed increased colocalization with EEA1 after depletion of CHC17 or SNX1 (Fig. 5, D and F; and quantified in Fig. 5 G). In contrast, CI-MPR did not display increased association with EEA1 after CHC22 depletion (Fig. 5, E and G). EEA1 itself displayed little overall change in CHC22-depleted cells, although a tendency for tubulation of $EEA1^+$ structures was noted. Thus, in endosomal sorting of CI-MPR, CHC22 appears to act downstream of early endosome exit and separately from CHC17.

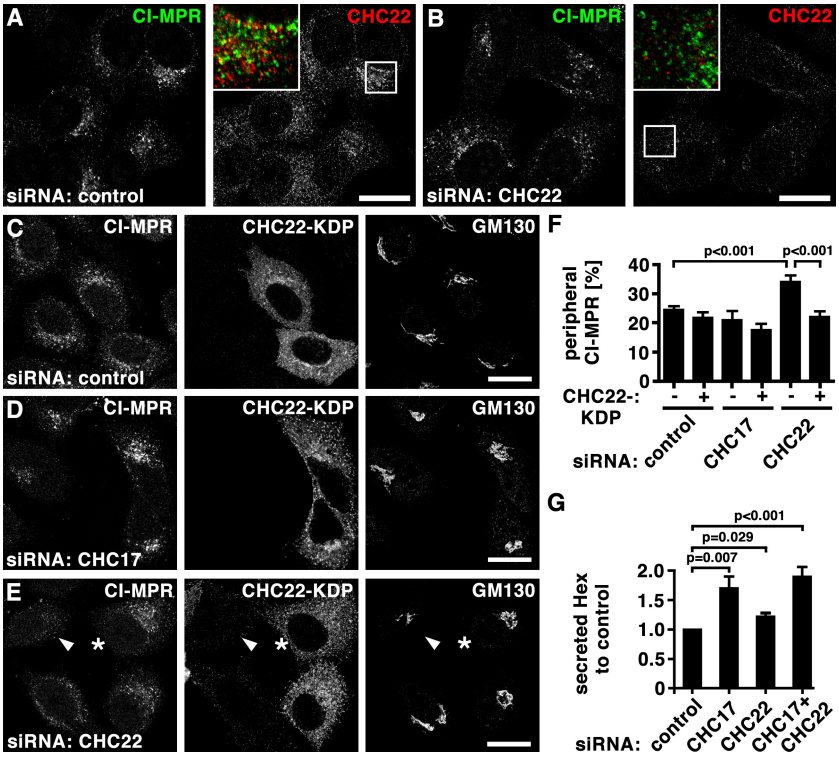

Figure 4. **CHC22 depletion leads to dispersal of CI-MPR from the perinuclear region.** (A and B) HeLa cells treated with control siRNA (A) or siRNA to deplete CHC22 (B) were processed for immunofluorescence and labeled for CI-MPR (green in merged insets) and CHC22 (red in merged insets) as indicated. Bars, 20 µm. (C–E) HeLa cells treated with control siRNA (C) or siRNA to deplete CHC17 (D) and CHC22 (E) were transfected with an siRNA-resistant, FLAG-tagged CHC22 construct (CHC22-KDP, knock-down proof), processed for immunofluorescence, and labeled for CI-MPR, FLAG-tag, and GM130 as indicated. In E, an asterisk marks a cell transfected with CHC22-KDP and siRNA targeting CHC22 that exhibits a normal concentration of CI-MPR in the perinuclear region, whereas an adjacent cell without CHC22-KDP (arrowhead) has dispersed CI-MPR, as in B. Bars, 20 µm. (F) For cells treated as in C–E, peripheral CI-MPR was quantified around the Golgi region (labeled with GM130) as a percentage of total CI-MPR, using the method illustrated in Fig. S4 (control cells: $n = 12$ for transfected and nontransfected; CHC17-depleted cells: $n = 7$ for nontransfected, $n = 12$ for transfected; CHC22-depleted cells: $n = 16$ for nontransfected, $n = 17$ for transfected; all cells from two independent experiments). Average percentages were plotted ± SEM. P-values for selected samples are indicated. (G) HeLa cells were treated with siRNAs against CHC17, CHC22, or a combination, or with control siRNA, as indicated below each bar, and hexosaminidase (Hex) activity was measured. Depicted is the ratio of extracellular to intracellular hexosaminidase activity for each treatment condition normalized to the ratio measured for control-treated cells in each experiment ($n = 5$, ±SEM shown). P-values for selected samples are indicated.

In contrast to CI-MPR cycling, TGN46 traffics rapidly from early endosomes to the TGN via recycling endosomes (Banting et al., 1998; Ganley et al., 2008; Nokes et al., 2008). This results in steady-state perinuclear accumulation in control cells (Fig. 6 A). TGN46 localization was not affected in CHC22-depleted cells (Fig. 6 C), whereas loss of CHC17 resulted in diminished and dispersed TGN46 labeling. This phenotype suggested retention of TGN46 in early endosomes and subsequent degradation in cells depleted of CHC17, correlating with reduced protein levels in these cells (Fig. 6 D). Thus, dependence of TGN46 traffic on CHC17 and independence from CHC22 function further distinguishes trafficking steps mediated by the two CHCs.

Shiga toxin B-subunit (STxB) serves as a model cargo for early endosome-to-TGN trafficking. Upon clathrin-independent entry into cells, STxB transits EEA1-positive early endosomes where it is sequentially sorted in CHC17- and retromer-dependent steps, before it is targeted to the TGN (Saint-Pol et al., 2004; Bujny et al., 2007; Popoff et al., 2007; Johannes and Popoff, 2008). In cells depleted of either CHC or SNX1, or in cells treated with control siRNA, STxB internalized for 15 min was colocalized with EEA1 (Fig. S5, A–D), indicating no defect in plasma membrane uptake. After 60 min of uptake, STxB showed perinuclear localization in control-treated cells (Fig. 7 A, Fig. S5 E), reproducing described kinetics for TGN arrival (Mallard et al., 1998). In cells depleted for either CHC or SNX1, STxB was more disperse, as though its retrograde transport to the TGN was impaired (Fig. 7, B–D, Fig. S5, F–H). Quantification of proximity to GM130 showed that peripheral STxB localization was more than doubled compared with its normal distribution in all three depletion conditions (Fig. 7 E). However, in CHC22-depleted cells, STxB was less colocalized with EEA1 (Fig. 7, C and F) than in cells depleted for CHC17 or SNX1 (Fig. 7, B, D, and F). Increased colocalization between STxB and EEA1 in CHC17- or SNX1-depleted cells was as expected, based on previous studies (Saint-Pol et al., 2004; Popoff et al., 2007). Thus, depletion of CHC22 did not affect STxB exit from the early endosome, where STxB was localized after 15 min of uptake (Fig. S5, A–D) and is sorted by CHC17 and SNX1. Instead, CHC22 depletion interfered with a later sorting step needed for endosome-to-TGN traffic of STxB, separating it from CHC17 function in this pathway, as well as in CI-MPR transport.

Examination of STxB, CI-MPR, and EEA1 together (Fig. 8) confirmed that both cargoes were able to transit from early endosomes after CHC22 depletion and were colocalized in a compartment (Fig. 8, C and E) with less EEA1 (Fig. 5 G and Fig. 7 F) compared with their localization after depletion of CHC17 or SNX1. After SNX1 depletion, both cargoes were colocalized with each other to the same extent as seen with CHC22 depletion (Fig. 8, D and E), but were increasingly localized with EEA1 (Fig. 5 G and Fig. 7 F), reflecting a common dependence on SNX1 for early endosome exit. CHC17 depletion, on the other hand, differentially affected the two cargoes. CI-MPR and STxB were less colocalized after CHC17 depletion than after CHC22 or SNX1 depletion (Fig. 8, B and E), and there was more overlap between STxB and EEA1 than between CI-MPR and EEA1 in CHC17-depleted cells (Fig. 7 F and Fig. 5 G). This can be

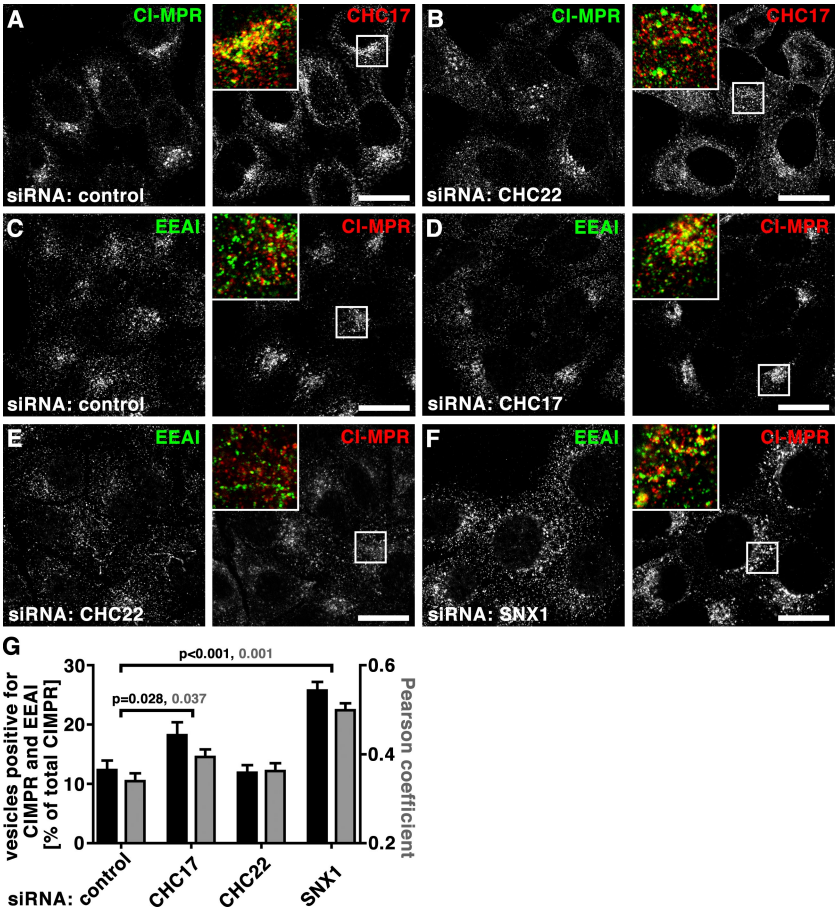

Figure 5. **Dispersed CI-MPR shows less association with early endosomes upon CHC22 depletion than after CHC17 or SNX1 depletion.** (A and B) HeLa cells treated with control siRNA (A) or siRNA targeting CHC22 (B) were processed for immunofluorescence and labeled using antibodies against CI-MPR (green in merged insets) and CHC17 (red in merged insets) as indicated. (C–F) Examples of cells quantified in G. HeLa cells treated with control siRNA (C) or siRNA to deplete cells of CHC17 (D), CHC22 (E), or SNX1 (F) were processed for immunofluorescence and labeled using antibodies against EEA1 (green in merged insets) and CI-MPR (red in merged insets) as indicated. Bars, 20 µm. (G) Vesicles containing both CI-MPR and EEA1 or only CI-MPR in cells depleted of the indicated proteins were automatically counted. The percentage of vesicles with double labeling was calculated relative to all vesicles containing CI-MPR for individual cells (n = 15 for control, n = 20 for CHC17-depleted, n = 25 for CHC22-depleted, n = 16 for SNX1-depleted cells; cells from two independent experiments). Average percentages ± SEM are shown in black against the left y-axis. Pearson coefficients of colocalization were determined for individual cells from the same experiments and plotted ± SEM (gray bars) against the right y-axis (n = 12 for each control and depletion condition, derived from two independent experiments). P-values for selected evaluation are indicated according to color code.

explained by a requirement for CHC17 in CI-MPR exit from the TGN that has been previously demonstrated (Hinrichsen et al., 2003). Thus, CHC22 function is required after early endosome exit of either cargo and before the divergence of STxB from CI-MPR on their respective routes to the TGN from endosomes. In complete distinction, CHC17 function is critical for CI-MPR export from the TGN, sorting of STxB (and some CI-MPR, e.g., Fig. 5 G) out of early endosomes, and recycling of TGN46 from endosomes to the TGN (Fig. 6). The CHC22-dependent step that commonly affects CI-MPR and STxB before their known retrograde divergence subdivides retrograde sorting, defining a novel stage in the endosomal transport pathway.

CHC22 plays a role in endosomal sorting in human myoblasts

Having localized CHC22 function to a distinct sorting step in the endosomal pathway in nonmuscle cells, it was of interest to determine if CHC22 plays the same role in myoblasts. In doing so, the issue of whether CHC22-dependent endosomal sorting is an important step in GLUT4 sequestration in the GSC is addressed (Hou and Pessin, 2007; Huang and Czech, 2007; Vassilopoulos et al., 2009). The human myoblast cell line LHCNM2 has a 1.5-fold higher ratio of CHC22 expression relative to CHC17 than HeLa (Fig. 1 B), and differentiates into myotubes, like the commonly studied rodent myoblast lines C2C12 and L6

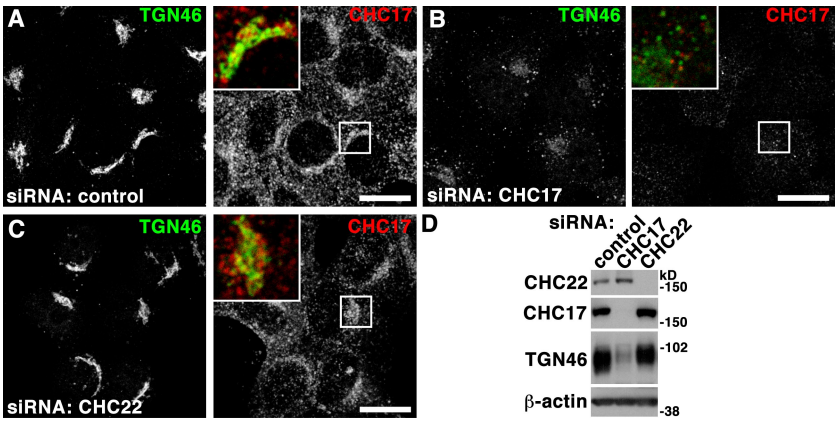

Figure 6. **CHC17 but not CHC22 depletion affects TGN46 distribution and trafficking.** (A–C) HeLa cells treated with control siRNA (A) or siRNA to deplete CHC17 (B) or CHC22 (C) were processed for immunofluorescence and labeled using antibodies against TGN46 (green in merged insets) and CHC17 (red in merged insets) as indicated. Bars, 20 µm. (D) Detergent lysates of HeLa cells treated with control siRNA or siRNA to deplete CHC17 or CHC22 as indicated at the top were separated by SDS-PAGE and immunoblotted with antibodies against the proteins indicated at the left. β-Actin serves as loading control.

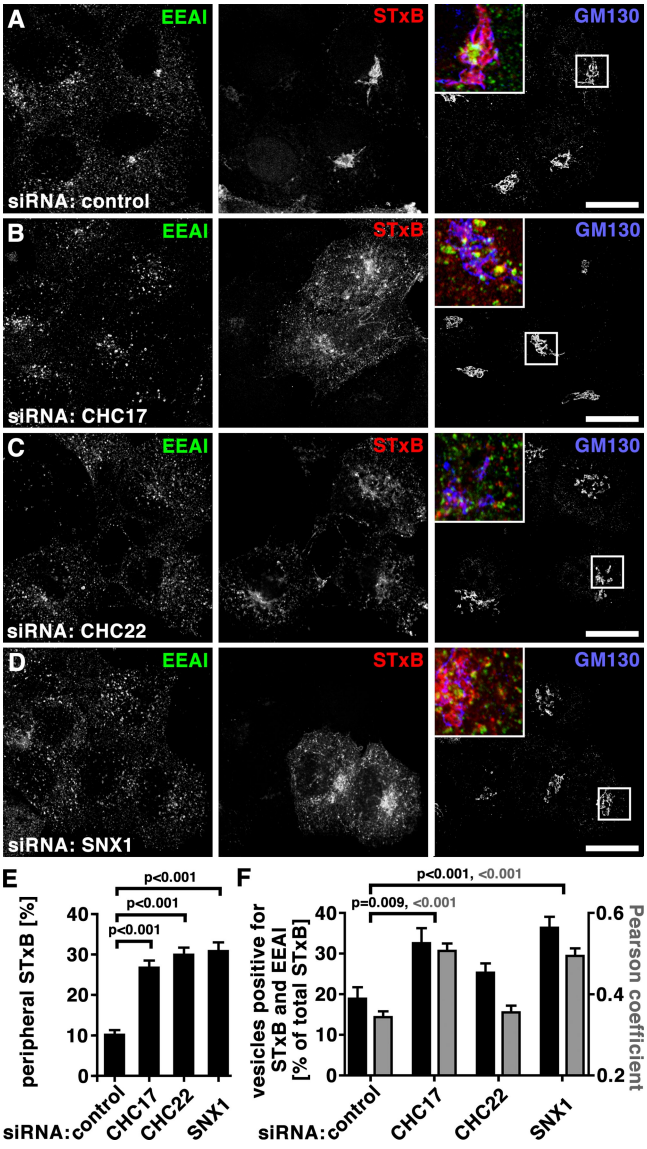

Figure 7. **Depletion of CHC17, CHC22, or SNX1 affects STxB trafficking.** (A–D) HeLa cells were treated with control siRNA (A) or siRNA to deplete cells of CHC17 (B), CHC22 (C), or SNX1 (D). Fluorescent STxB (red in merged insets) in fresh medium was bound to cells for 30 min on ice, washed in PBS, and chased for 60 min in fresh medium at 37°C. Cells were fixed, processed for immunofluorescence, and labeled using antibodies against EEA1 (green in merged insets) and GM130 (blue in merged insets). Bars, 20 µm. (E) Peripheral STxB signal around the Golgi (detected by GM130 labeling) was determined in cells treated as in A–D. Peripheral signals were calculated as percentages of total signal from individual cells using the method illustrated in Fig. S4 (n = 20 each for control, CHC17-depleted, CHC22-depleted, and SNX1-depleted cells; cells from two independent experiments) and average percentages were plotted ± SEM. P-values for selected samples are indicated. (F) Vesicles containing both STxB and EEA1 or only STxB in cells depleted of the indicated proteins were automatically counted. The percentage of vesicles containing double labeling relative to all vesicles containing STxB was calculated for individual cells (n = 15 for control, n = 20 for CHC17-depleted, n = 25 for CHC22-depleted, n = 16 for SNX1-depleted cells; cells from two independent experiments). Average percentages are shown ± SEM in black against the left y-axis. Pearson's coefficients of colocalization were determined for cells from the same experiments and plotted ± SEM (gray bars) against the right y-axis (n = 12 for the control and each of the depletion conditions from two independent experiments). P-values for selected evaluation are indicated according to color code.

(Zhu et al., 2007). Depletion of CHC22 or CHC17 from LHCNM2-derived myotubes (Fig. 9, A–D) had similar effects to those observed for HeLa cells (Fig. 5). In myotubes depleted of CHC22, CI-MPR was dispersed compared with its perinuclear focus around myonuclei in control-treated myotubes. This strong CI-MPR association with myonuclei made it hard to quantify a qualitatively denser appearance upon CHC17 depletion. However CI-MPR labeling was clearly different in myotubes depleted for each CHC and, as seen for HeLa cells, a slight increase in CHC22 protein level was observed in CHC17-depleted cells (Fig. 9 E). CI-MPR-levels were decreased to 83% and 61% of control cells after depletion of CHC17 or CHC22, respectively (Fig. 9, E and F), confirming a role for both CHCs in influencing endosomal sorting of CI-MPR in myotubes. To address whether CHCs function at different steps of CI-MPR sorting, as in HeLa cells, processing of the CI-MPR–transported lysosomal hydrolase, Cathepsin D, was analyzed. Upon exiting the TGN as an immature protein (pro, 53 kD) bound to CI-MPR, Cathepsin D enters the endocytic pathway where it is proteolytically processed to an intermediate (pre) form (47 kD) and then into a mature form (31 kD). Levels of these Cathepsin D forms may be used to assess trafficking toward the lysosome (Mardones et al., 2007). After CHC22 depletion, the amount of intermediate (pre) form was increased (Fig. 9, E and G), indicative of Cathepsin D accumulation with CI-MPR in an intermediate endocytic compartment. This effect was not observed upon CHC17 depletion, consistent with the limited effect of CHC17 depletion on CI-MPR in muscle cells. Thus, CHC22 plays a role in endosomal sorting in muscle cells that is distinct from functions of CHC17, and is implicated in the same functional pathway as was mapped for CHC22 in HeLa cells.

GLUT4 targeting to the GSC in human muscle depends on CHC22 (Vassilopoulos et al., 2009), and the studies reported here map CHC22 function in muscle to retrograde endosomal transport. In mice, which normally do not express CHC22, transgenically introduced CHC22 interacts with adaptors responsible for GLUT4 transport and disrupts murine GLUT4 traffic such that the formation and function of the GSC is impaired. It is conceivable that for CHC22 to function as it does in humans, additional species-specific factors are needed to complete its role in GSC formation (Vassilopoulos et al., 2009). An obvious candidate for such a factor is the SNARE family protein STX10, which plays a role in retrograde transport of CI-MPR from endosomes to the TGN, is enriched in muscle, and is expressed in humans but not mice (Tang et al., 1998; Ganley et al., 2008). The effects of STX10 depletion on GLUT4 traffic in human myoblasts were therefore assessed (Fig. 10) and found to phenocopy CHC22 depletion, causing dispersion and loss of GLUT4 staining (Fig. 10, B–D). As seen previously, STX10 depletion also caused dispersion of the CI-MPR in HeLa cells (Fig. 10 F), but it did not affect retrograde transport of STxB (Fig. 10 G; Mallard et al., 2002; Ganley et al., 2008). Again, phenocopying CHC22 (Vassilopoulos et al., 2009), STX10 depletion slightly reduced total GLUT4 levels in myotubes (Fig. 10, H and I), indicating that GLUT4 was partially degraded when GSC formation was disrupted. Localization of CHC22 was not severely affected in cells depleted of STX10 (Fig. 9 A, Fig. 10 C), whereas CHC22

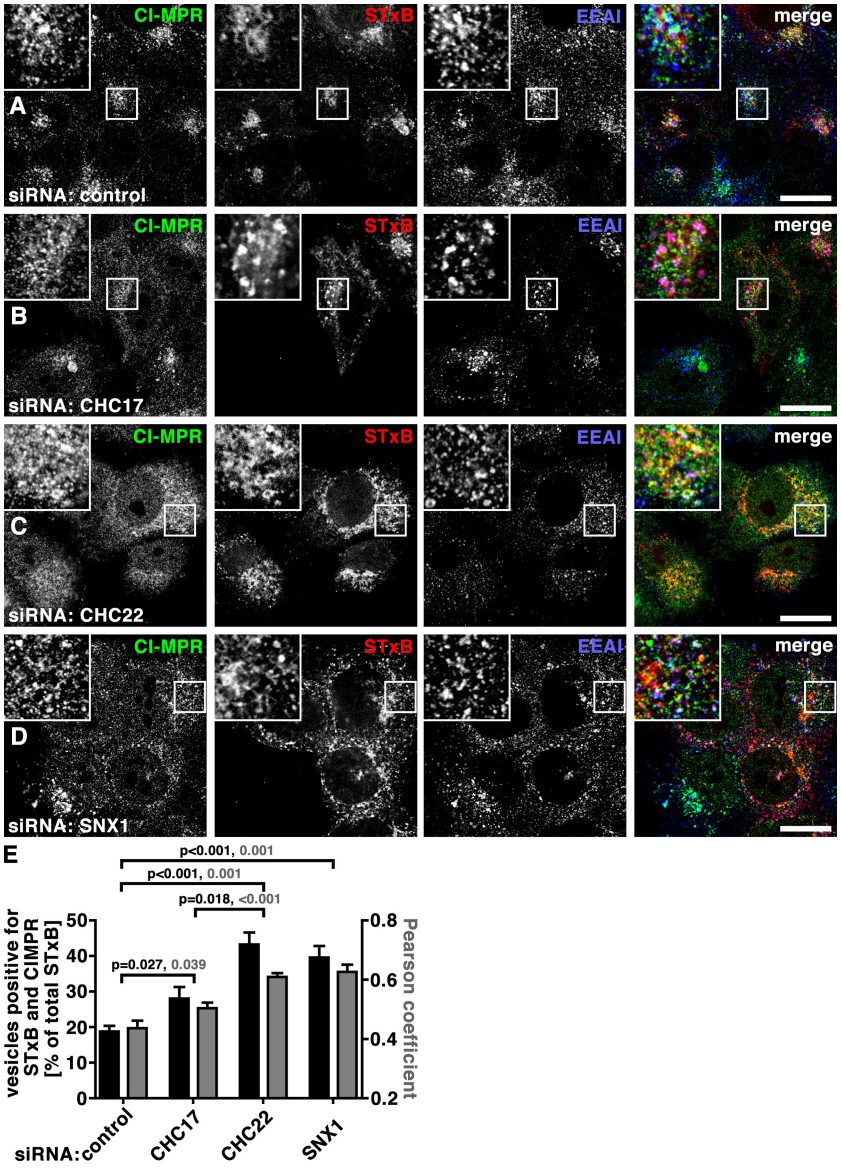

Figure 8. **Retrograde traffic of STxB and CI-MPR from endosome to TGN is differentially impaired in CHC17-, CHC22-, and SNX1-depleted cells.** (A–D) HeLa cells were treated with control siRNA (A) or siRNA targeting CHC17 (B), CHC22 (C), or SNX1 (D). Fluorescent STxB (red in merged insets) in fresh medium was bound to cells for 30 min on ice, washed in PBS, and chased for 60 min in fresh medium at 37°C. Cells were fixed, processed for immunofluorescence, and labeled using antibodies against CI-MPR (green in merged insets) and EEA1 (blue in merged insets). Bars, 20 µm. (E) Vesicles containing both STxB and CI-MPR or STxB only were automatically counted in cells depleted of the indicated proteins. The percentage of vesicles containing double labeling relative to all vesicles containing STxB was calculated for individual cells (n = 15 for control, n = 20 for CHC17-depleted, n = 25 for CHC22-depleted, n = 16 for SNX1-depleted cells; cells from two independent experiments). Average percentages are shown ± SEM in black against the left y-axis. Pearson's coefficients of colocalization were determined for cells from the same experiments and plotted ± SEM (gray bars) against the right y-axis (n = 12 for the control and each of the depletion conditions from two independent experiments). P-values for selected evaluation are indicated according to color code.

depletion led to some dispersion of STX10 (Fig. 10, A and D). This suggests that CHC22 acts upstream of STX10 in endosomal sorting, consistent with CHC22 depletion affecting all three cargoes but STX10 depletion affecting only CI-MPR and GLUT4, but not STxB trafficking. Targeting STxB to the TGN must precede that of the other two cargoes, further subdividing retrograde transport from endosomes to TGN into two steps that follow a novel CHC22-dependent step. These data, which establish the joint participation of CHC22 and STX10 in GLUT4 traffic, map endosomal sorting and retrograde endosome-to-TGN transport as critical steps in GSC formation in human tissue.

Discussion

In this study we define the membrane-trafficking function of CHC22, a second isoform of the clathrin heavy chain, which is present in humans in addition to the CHC17 isoform. We found that CHC22 is expressed at variable levels in all human cells studied and establish that CHC22 has a ubiquitous function needed for endosomal sorting of both exogenous (STxB) and endogenous (CI-MPR, GLUT4) vesicle cargo. This localizes the normal intracellular function of CHC22, which is completely distinct from that of CHC17, and defines a novel stage in retrograde endosome-to-TGN sorting.

CHC17 and CHC22 sequences differ in key functional regions mediating CLC association and adaptor interactions (Wakeham et al., 2005), such that endogenous CHC22 does not bind either AP2 or CLCs in cells. Instead, the region that binds CLCs in CHC17 mediates SNX5 interaction for CHC22 (Liu et al., 2001; Towler et al., 2004; Vassilopoulos et al., 2009). Depletion of each CHC leads to completely different phenotypes with respect to endosomal sorting, TGN sorting, and endocytosis (Figs. 1, 4–8, and Fig. S5) in Hela cells and additionally GSC formation in skeletal muscle (Fig. 9 and Fig. 10; Vassilopoulos et al., 2009). Sequence divergence between CHCs is not solely responsible for their functional divergence, as abnormally high levels of CHC22 may rescue CHC17 function when CHC17 is depleted (Hood and Royle, 2009). However, endogenous CHC22

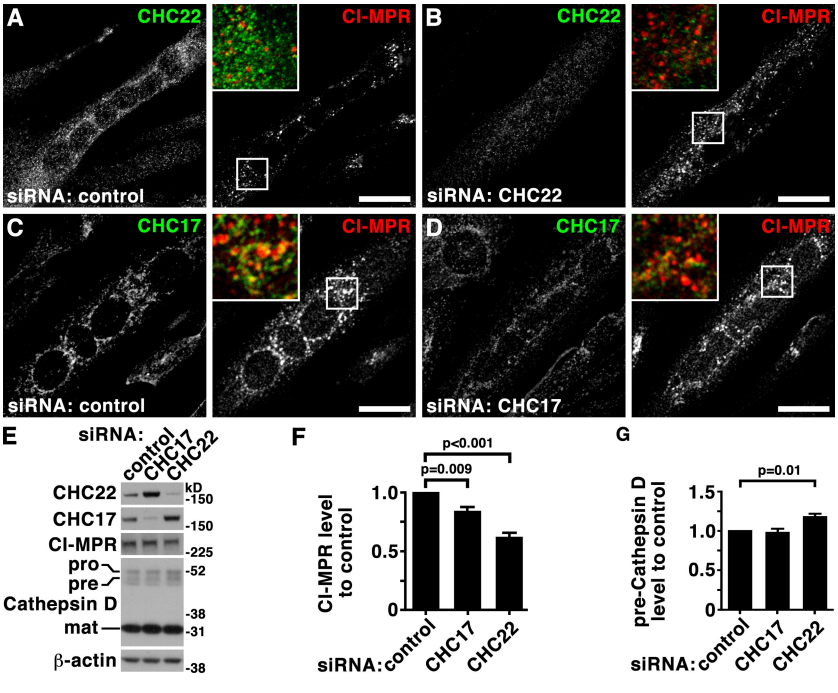

Figure 9. **Effects of CHC17 and CHC22 down-regulation on CI-MPR trafficking in human myoblasts reproduce effects in HeLa cells.** (A–D) LHCNM2 human skeletal muscle myoblasts were differentiated, treated with control siRNA (A and C) or siRNA targeting CHC22 (B) or CHC17 (D) and processed for immunofluorescence. Cells were double labeled using antibodies against CHC17 (green in merged insets), CHC22 (green in merged insets), and CI-MPR (red in merged insets) as indicated. Bars, 20 µm. (E) LHCNM2 cells were differentiated and treated with siRNA targeting CHC17 or CHC22 or control siRNA as indicated at the top of each lane. Whole-cell detergent lysates were separated by SDS-PAGE and immunoblotted with antibodies against the proteins indicated at the left. Immature (pro), intermediate (pre), and mature (mat) forms of Cathepsin D are indicated at the left. β-Actin serves as a loading control. (F) Quantification of CI-MPR levels in whole-cell detergent lysates from siRNA-treated cells generated as in E. Shown are levels ± SEM in the samples treated with the specific siRNA indicated under each bar compared with levels in cells treated with control siRNA in the same experiment ($n = 5$). P-values for selected samples are indicated. (G) Quantification of preCathepsin D levels in whole-cell detergent lysates from siRNA treated cells generated as in E. Shown are levels ± SEM in the samples treated with the specific siRNA indicated under each bar compared with levels in cells treated with control siRNA in the same experiment ($n = 5$). P-values for selected samples are indicated.

protein levels are at least eightfold lower than CHC17 levels in cells (Fig. 1), such that complete functional separation is ensured. Even in the context of variable CHC17 surplus, CHC22 binds its own subset of AP1 and AP3 adaptors on endosomes, possibly assisted by SNX5 or GGA interaction (Fig. 3; Figs. S1–S3) (Towler et al., 2004; Vassilopoulos et al., 2009). Hence, the segregation of CHC functions that emerged after gene duplication (Wakeham et al., 2005) is dictated by their sequence divergence as well as their relative concentration in cells, such that CHC22 cannot outcompete CHC17 but also has its own unique interactions.

The studies reported here demonstrate that CHC22 function is required for endosomal sorting that occurs after the CHC17-dependent step required for retrograde cargo exit from early endosomes (Saint-Pol et al., 2004) and early retrograde transport of TGN46 (Figs. 4–8). CHC17 and the retromer complex act sequentially in STxB export from the early endosome to later stages of the retrograde pathway and are proposed to play the same role for CI-MPR (Johannes and Popoff, 2008). Accordingly, for both cargoes, depletion of the retromer component SNX1 had a similar phenotype to CHC17 depletion but different from CHC22 depletion, placing CHC22 downstream of this particular retromer function. STxB does not progress to the lumen of late endosomes before its retrograde transport to the TGN (Mallard et al., 1998; Saint-Pol et al., 2004), whereas CI-MPR at least partially does (Lombardi et al., 1993; Ganley et al., 2008; Seaman et al., 2009). The accumulation of CI-MPR and STxB in the same compartment in cells depleted of CHC22 suggests that these two cargoes exit early endosomes together and that subsequent CHC22-dependent traffic and/or sorting occurs before they diverge. The SNARE family member STX10, which has been implicated in fusion processes at both TGN and endosomal membranes (Ganley et al., 2008), likely functions downstream of CHC22 in retrograde transport (Fig. 10). Collectively, the data presented here indicate a sequential sorting process for CI-MPR and STxB involving first CHC17 and retromer mediating exit of both cargoes from the early endosome, then requiring CHC22 function for a later retrograde sorting step affecting both STxB and CI-MPR. At this point, divergence of STxB and CI-MPR occurs with STxB directly trafficking to the TGN, but CI-MPR requiring subsequent STX10 and Rab9 functions for retrograde transport. Thus, CHC22-mediated sorting defines a novel intermediate stage of retrograde sorting that influences the fate of multiple cargoes and does not overlap with CHC17 function.

Retrograde sorting from the endocytic pathway requires tubulation from early endosomes, dependent on dynactin, CHC17, and recruitment of retromer (Popoff et al., 2007; He et al., 2008; Rojas et al., 2008; Seaman et al., 2009; Wassmer et al., 2009). We propose that like CHC17, CHC22 function may also involve retromer. SNX5, a component of the retromer complex, can bind CHC22 and is detected on the tubular sorting compartment from which later retrograde transport involving CHC22 would emerge (Wassmer et al., 2009). CHC22 could be actively sorting cargo or mediate a sorting step that influences compartment composition and thereby affects its function, analogous to the role defined for CHC17 (Arighi et al., 2004; Saint-Pol et al., 2004; Seaman, 2004; Bujny et al., 2007; Popoff et al., 2007; Johannes and Popoff, 2008). Despite our best efforts, it has not yet been possible to localize endogenous CHC22 by electron microscopy to establish whether it is primarily associated with tubules, vesicles, or larger endocytic compartments. We did, however, observe that depletion of CHC22 increased endosome tubulation (Fig. 5 E) and previously observed that transfected CHC22 localized to

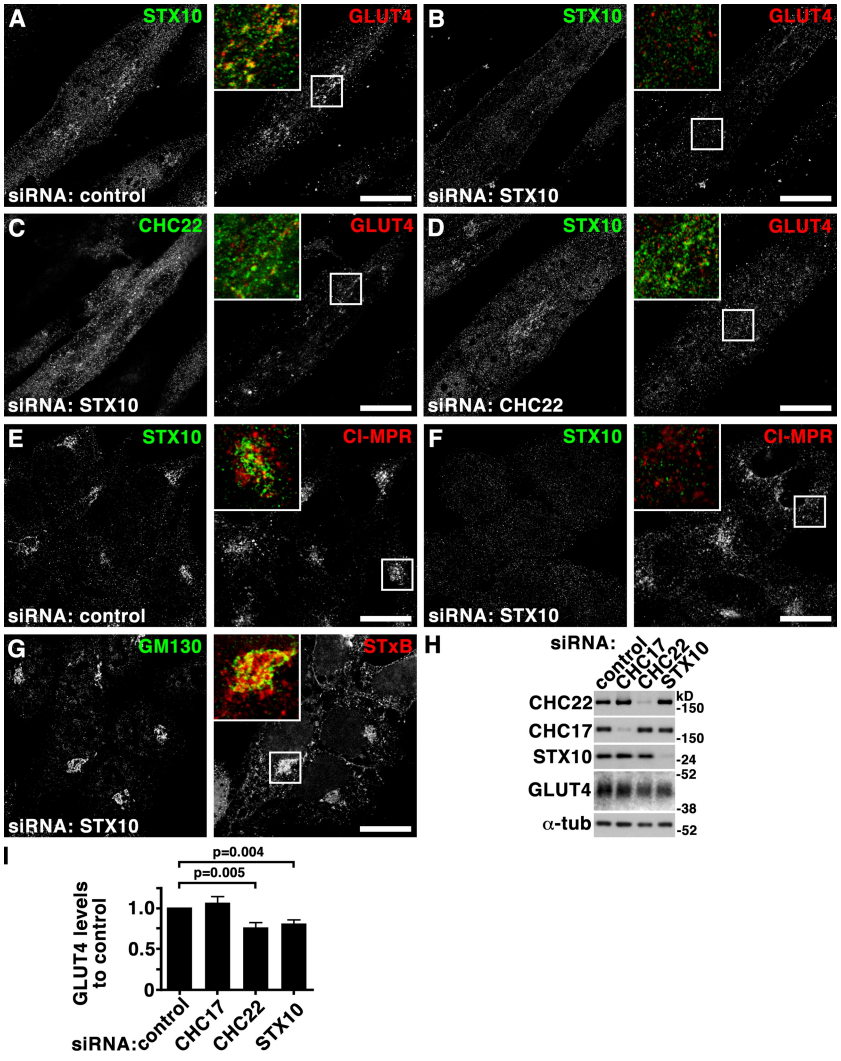

Figure 10. **Syntaxin 10 depletion partially phenocopies CHC22 depletion and is implicated in GLUT4 sequestration.** (A–D) LHCNM2 human skeletal muscle myoblasts were differentiated, treated with control siRNA (A) or siRNA targeting STX10 (B and C) or CHC22 (D), and processed for immunofluorescence. Cells were double labeled using antibodies against STX10 (A, B, and D; green in merged insets), CHC22 (C; green in merged inset), and GLUT4 (red in merged insets) as indicated. Bars, 20 µm. (E–G) HeLa cells treated with control siRNA (E) or siRNA to deplete STX10 (F and G) levels were processed for immunofluorescence and labeled for STX10 (E and F; green in merged insets) and CI-MPR (E and F; red in merged insets) as indicated at the top. In G, fluorescent STxB (red in merged inset) in fresh medium was bound to cells for 30 min on ice, washed in PBS and chased for 60 min in fresh medium at 37°C, fixed, and processed for immunofluorescence using antibodies against GM130 (green in merged insets). (H) Detergent lysates of LHCNM2 cells treated with siRNA to deplete CHC17, CHC22, or STX10 or with control siRNA as indicated at the top were separated by SDS-PAGE and immunoblotted with antibodies against the proteins indicated at the left. α-Tubulin (α-tub) serves as a loading control. (I) Quantification of GLUT4 levels in detergent lysates of siRNA-treated cells generated as in H. Shown are levels ± SEM in the samples treated with the specific siRNA indicated under each bar compared with levels in cells treated with control siRNA in the same experiment (n = 6). P-values for selected samples are indicated.

vesicles in the TGN (Liu et al., 2001). Notably, our data indicate that formation of the compartment where CHC22 functions depends on CHC17 function early in the endocytic pathway. This explains why proteomic analysis of vesicle proteins that disappear from membrane preparations after CHC17 depletion included CHC22 (Borner et al., 2006).

The membrane traffic of GLUT4 to the insulin-regulatable GSC and CHC contribution to GSC formation has been characterized in rodent and human muscle and fat cells (Shewan et al., 2003; Karylowski et al., 2004; Li and Kandror, 2005; Hou and Pessin, 2007; Huang and Czech, 2007; Antonescu et al., 2008; Williams and Pessin, 2008; Fazakerley et al., 2009; Vassilopoulos et al., 2009). Here, we demonstrate that CHC22, in conjunction with STX10, influences retrograde transport and in human skeletal muscle both proteins contribute to GSC formation. Although our findings show that endosomal sorting and a retrograde endosome–TGN pathway are critical for human GSC formation, they cannot definitively answer whether, after CHC22 and STX10 action, GLUT4 is trafficked to the GSC via the TGN or from an endosomal compartment.

The GLUT4 pathway, although restricted to muscle and fat, depends on ubiquitously expressed molecules that mediate membrane traffic in other cell types. While playing a role in nonmuscle cells, both CHC22 and STX10 are enriched in muscle (Fig. 1; Sirotkin et al., 1996; Tang et al., 1998), likely contributing to specialization of the GLUT4-trafficking pathway. Although showing similar tissue distribution and species restriction, as well as shared depletion phenotypes with respect to CI-MPR and GLUT4 targeting, CHC22 and STX10 differ in their contribution to STxB trafficking. STX10 depletion does not affect STxB transport and a slight but detectable effect of CHC22 depletion on STX10 localization places STX10 downstream of CHC22 function in retrograde sorting. These findings suggest that CHC22 function is required for STX10 targeting and sorting. Additionally, the SNARE STX10 may be required for fusion of GLUT4-containing vesicles that are formed as a result of CHC22 function. Indeed, transgenic mice expressing human CHC22 (without STX10) accumulate membrane compartments filled with GLUT4, which apparently do not fuse with target membranes, leading to a dampened insulin response in these animals (Vassilopoulos et al., 2009).

The remarkable absence of both CHC22 and STX10 from the mouse genome (Wakeham et al., 2005; Ganley et al., 2008) has the consequence that GLUT4 traffic differs in humans and

mice. The basic pathways and sorting signals for GLUT4 trafficking are likely to be the same in the two species, but the presence of CHC22 and STX10 apparently modulates the balance between compartments where GLUT4 resides, and thereby influences the degree of GLUT4 sequestration in the GSC. Consistent with less efficient GSC formation, mice display characteristic differences in their glucose homeostasis compared with humans. After a meal, the main pathway for glucose uptake in humans is through the insulin-regulatable GLUT4 pathway in skeletal muscle, whereas mice rely more heavily on insulin-stimulated reduction of glucose release from the liver (Brüning et al., 1998; Shepherd and Kahn, 1999; Michael et al., 2000). The mouse obviously adapted to loss of CHC22 and STX10, and the induction of diabetic symptoms in CHC22-transgenic mice suggests that the presence of one protein without the other is not favorable to mouse metabolism. The expanded GSC in some patients with type 2 diabetes has high levels of CHC22 associated with it (Vassilopoulos et al., 2009), raising the possibility that CHC22 modulation of GLUT4 traffic might influence human tendency toward type 2 diabetes. Thus, to study human diabetes in mouse models, the roles of both CHC22 and STX10 will have to be recapitulated. One exciting possibility is that the coexpression of these proteins might induce a human-like GSC in mice, leading to better mouse models of human glucose metabolism.

Materials and methods

Expression plasmids, antibodies, recombinant proteins, and siRNAs

Full-length human CHC22 was cloned from LHCNM2 skeletal muscle cells. mRNA was extracted using the RNeasy kit (QIAGEN) and transcribed into cDNA using SuperScript (Invitrogen). CHC22 was cloned into pT7blue cloning vector and subcloned into pEGFP-C1 and p3xFLAG-CMV-10 vectors for expression in HeLa cells. siRNA-resistant FLAG-CHC22-KDP was generated by QuikChange mutagenesis (Agilent Technologies) using primers CAACAACTGGGAGGATTTGGTGAAATTTCTGCAGATG and CATCTGCAGAAATTTCACCAAATCCTCCCAGTTGTTG on CHC22 in p3xFLAG-CMV-10, resulting in three base changes without changing the amino acid sequence.

One monoclonal and two polyclonal antibodies that specifically recognize CHC22 and not CHC17 have been described previously (Liu et al., 2001; Vassilopoulos et al., 2009). Anti-CHC17 antibodies (mouse monoclonals X22 and TD.1) and rabbit polyclonal antibody against clathrin light chains were generated in the Brodsky laboratory (Brodsky, 1985; Acton et al., 1993). Commercial sources of antibodies are as follows: TGN46 (sheep polyclonal; AbD Serotec); EEA1, AP1, SNX1, GM130 (mouse monoclonal; BD); α-tubulin, β-actin, FLAG (mouse monoclonal; Sigma-Aldrich); EEA1 (rabbit polyclonal; Cell Signaling Technology); GM130 (rabbit polyclonal, Sigma-Aldrich); CI-MPR (mouse monoclonal, EMD); Cathepsin D (rabbit polyclonal; EMD); and SNX5 (goat polyclonal; Abcam). Mouse monoclonal anti-Rab9 and rabbit polyclonal anti-STX10 antibodies were gifts from Suzanne Pfeffer (Stanford University School of Medicine, Stanford, CA). Polyclonal anti–CI-MPR was a gift from Linton Traub (University of Pittsburgh, Pittsburgh, PA). The Rab11-GFP construct was a gift from Keith Mostov (University of California, San Francisco, San Francisco, CA). Secondary antibodies for immunofluorescence against mouse IgG, IgG1, IgG2a, rabbit IgG, sheep IgG, and goat IgG were from Invitrogen (Alexa Fluor 488, 555, 568, and 647 conjugates). Secondary antibodies coupled to HRP were from Invitrogen. Recombinant STxB coupled to Cy3 was produced as described previously (Mallard et al., 1998).

Targeting and nontargeting control siRNAs were synthesized by QIAGEN. DNA sequences targeted were AATTCTCCGAACGTGTCACGT for nontargeting control, AAGCAATGAGCTGTTTGAAGA for CHC17 (Huang et al., 2004), AAGAACAAGACCAAGAGCCAC for SNX1 (Bujny et al., 2007), TATCCCACATGACGAGTGA for STX10 (Ganley et al., 2008), and TCGGGCAAATGTGCCAAGCAA and AACTGGGAGGATCTAGTTAAA for CHC22 (1:1 mixture of siRNAs were used; Vassilopoulos et al., 2009). In experiments shown in Fig. 4 E only the second siRNA against CHC22 was used, and the depletion efficiency was comparable to results using the siRNA mixture, as judged by immunoblotting whole-cell detergent lysates.

Cell culture

HeLa 229, MDA231, A431, HEK 293, HFF, HepG2, JR1, and C2C12 cells were grown in DME supplemented with 10% FBS, 50 U/ml penicillin, 50 µg/ml streptomycin, and 0.625 µg/ml fungizone. NKL natural killer cells were grown in RPMI 1640 supplemented with 10% FBS, 200 U/ml IL2, 50 U/ml penicillin, and 50 µg/ml streptomycin. LHCNM2 human skeletal muscle cells (Zhu et al., 2007) were maintained in tissue culture flasks coated with rat-tail collagen in basal medium (4:1 DME/M199, 0.02 M Hepes, 0.03 µg/ml $ZnSO_4$, and 1.4 µg/ml vitamin B12) with 15% fetal bovine serum (FBS), 55 ng/ml dexamethasone, 2.5 ng/ml hepatocyte growth factor (Sigma-Aldrich), 50 U/ml penicillin, 50 µg/ml streptomycin, and 0.625 µg/ml fungizone (growth medium). Differentiation was induced by culturing in fusion medium (basal medium with 0.5% FBS, 10 µg/ml insulin, 50 µg/ml apo-transferrin, and 5.5 ng/ml dexamethasone) followed by differentiation medium (basal medium with 0.5% FBS and 55 ng/ml dexamethasone).

Cells were transfected with 10 nM siRNA using HiPerfect (QIAGEN) according to the manufacturer's instructions. HeLa cells were split, reseeded 24 h after transfection, and retreated with siRNA 24 h later. Cells were used for experimentation 48–72 h after the second round of transfection. LHCNM2 cells were transfected twice, 72 h apart, and used 72 h later. For plasmid transfection Lipofectamine 2000 (Invitrogen) was used according to the manufacturer's instructions 24 h before analysis of transfected cells.

Internalization assays

For internalization assays cells were grown on coverslips and transfected with siRNA as described above. STxB uptake was performed as described previously (Popoff et al., 2007). In brief, cells were washed twice in cold PBS on ice and incubated on ice in prechilled medium containing 2 µg/ml STxB coupled to Cy3 for 30 min. Cells were then washed twice in cold PBS on ice and taken off ice. Warm media was added and cells were incubated at 37°C for various times before fixation. For transferrin internalization, cells were washed twice in warm PBS and preincubated for 45 min at 37°C in DME supplemented with 0.02M Hepes and 1% BSA (serum-free media [SFM]) to allow for recycling of the intracellular receptor. Cells were then washed twice in cold PBS on ice and incubated on ice for 30 min in prechilled SFM containing 10 µg/ml transferrin coupled to Alexa Fluor 488 (Invitrogen). After washing twice in cold PBS on ice, cells were taken off ice and warm medium was added. Cells were then incubated at 37°C for 10 min before fixation.

Hexosaminidase secretion

Hexosaminidase secretion was measured using a protocol modified from one described previously (Riederer et al., 1994). Cells treated with siRNA as described above were washed in PBS and incubated in DME supplemented with 10 mM mannose-6-phosphate for 8 h at 37°C. Secreted hexosaminidase activity was assayed in 0.5 ml medium by addition of 120 µl 5x hexosaminidase substrate buffer (0.5 M sodium acetate, pH 4.4, 0.5% Triton X-100, and 5 mM *p*-nitrophenyl-*N*-acetyl-β-D-glucosaminide). After shaking at 37°C for 1 h, reactions were stopped by addition of 0.6 ml stop buffer (0.5 M glycine and 0.5 M Na_2CO_3, pH 10.0). Release of *p*-nitrophenol was measured spectrophotometrically at 405 nm. Intracellular hexosaminidase was measured by washing the cells twice in cold scraping buffer (10 mM phosphate buffer, pH 6.0, and 0.15 M NaCl) and then scraping them into scraping buffer supplemented with 0.5% Triton X-100. After centrifugation at 100,000 *g* for 15 min at 4°C, 50 µl of the resulting supernatant was assayed in 570 µl 1x hexosaminidase substrate buffer. Secreted hexosaminidase was determined as the percentage of the total hexosaminidase for each sample (extracellular plus intracellular). Secreted hexosaminidase of samples treated with specific siRNA was then compared with that of samples treated with control siRNA and ratios were calculated. P-values were calculated using unpaired two-tailed Student's *t* test.

Immunoblotting

Protein samples were separated by SDS-PAGE (4–12% acrylamide gel; Invitrogen), transferred to nitrocellulose (Millipore) and labeled with primary antibodies at 1–5 µg/ml and peroxidase-conjugated secondary antibodies. The presence of antibody-labeled proteins in samples was detected using Western Lightning Chemiluminescence Reagent (GE Healthcare). Rainbow molecular weight markers (GE Healthcare) were used to assess transfer efficiency and judge protein sizes. The migration positions of molecular weight marker proteins are indicated in kilodaltons (kD) at the right of each blot presented. Quantification was performed using Quantity One software (Bio-Rad Laboratories). To calibrate antibody blotting signals for quantification

of CHC levels, dilutions of cell lysates were analyzed on the same gel as dilutions of recombinant protein fragments representing portions of CHC22 (amino acids 1521–1640) and CHC17 (1–1074) containing the blotting antibody epitopes. Gels were transferred to nitrocellulose and immunoblotted sequentially with polyclonal antibody against CHC22 and monoclonal antibody against CHC17, stripping in between. The dilutions of lysates and recombinant fragments analyzed were empirically selected to generate signals in a linear range. The generated antibody signals were plotted against protein concentration of material analyzed so that the CHC content of each lysate could be determined by comparison to the recombinant protein signals. The molar ratios of CHC22 to CHC17 in the cell lysates were then calculated, taking into account fragment length. All calculations and graphs were performed and generated in Microsoft Excel and GraphPad Prism software. P-values were calculated using unpaired two-tailed Student's *t* test.

Immunofluorescence and image analysis

Cells grown on coverslips were washed in warm PBS, fixed in warm PFA (3.7% in PBS, 10 min), then washed (2x, 5 min, PBS), permeabilized (4 min, 3% BSA, and 0.5% Triton X-100 in PBS), and blocked in blocking solution (3% BSA in PBS, 30 min). Antibody labeling was performed by inversion of coverslips on 20 µl blocking solution with primary or secondary antibodies (1–5 µg/ml), DAPI, or TO-PRO3 on parafilm and washing with PBS. Samples were mounted in the Prolong Antifade kit (Invitrogen). Images presented in Figs. 3 C; Fig. 5, A and B; Fig. S1, F and G; and Fig. S2, B and E were acquired by confocal laser scanning microscopy using a microscope system (EZ-C1Si; Nikon) equipped with a Plan-Apo 100x, 1.40 NA oil objective and 405-, 488-, and 561-nm laser lines. All other samples were analyzed using a microscope system (TCS SP5; Leica) with a 63x HCX Plan-Apo CS oil objective using 488-, 543-, and 633-nm laser lines. Imaging was performed at room temperature using Nikon immersion oil and Leica Type F immersion oil. DAPI, Alexa 488, Alexa 555, Alexa 568, Alexa 647, and TO-PRO3 fluorescence was sequentially excited using lasers with wavelengths of 405 (DAPI), 488 (Alexa 488), 543 (Alexa 555), 561 (Alexa 568), and 633 nm (Alexa 647, TO-PRO3). Images (1024 × 1024 pixels) were saved as TIFF files in NIS Elements software (Nikon), MetaMorph software (MDS Analytical Technologies), and Leica LAS AF software, and input levels were adjusted in Adobe Photoshop. Labeling detected in individual channels is presented in black and white in individual panels. 3x enlarged merged images of boxed areas are presented in color with labeling colors being color coded as described in accompanying figure legends. Overlap of red and green staining is yellow, overlap of red and blue staining is magenta, overlap of green and blue staining is turquoise, and overlap of all three channels is white.

Image quantification was performed using National Institutes of Health's ImageJ (http://rsb.info.nih.gov/ij). Colocalization of markers on vesicles in the periphery of double-labeled cells was performed after excluding the dense concentration of vesicles in the Golgi region because measuring individual vesicles is problematic in this area. Exclusion was the same for all cells and defined by a circular area of 72.2 μm^2 centered at the most dense point of the Golgi. For each cell, individual marker fluorescence was measured in separate channels, and signals were adjusted to their dynamic ranges. For each marker, only particles larger than 0.094 μm^2 (16 pixels) were automatically selected and counted. These automatically selected vesicles from individual labelings were then overlaid and colocalization was highlighted using the Colocalization Highlighter plugin (Pierre Bourdoncle, Institut Jacques Monod, Service Imagerie, Paris, France). The colocalized signal was again subjected to automatic particle count using the same automatic size exclusion as used to select individually labeled vesicles. The quotient of colocalized particles over total particles for one marker was calculated for individual cells and averaged.

Degree of overlap of markers in individual cells was determined by Pearsons' correlation coefficients and pixel shifts (van Steensel et al., 1996) to estimate colocalization as well as its specificity. Measurements were performed on total fluorescence of single cells using the JACOP plugin (Bolte and Cordelières, 2006).

To quantify peripheral and perinuclear fluorescence of CI-MPR and STxB, individual cells were analyzed using the radial profile plugin (Paul Baggethun; Hehnly et al., 2006; see also illustrative Fig. S4). Fluorescent intensities within individual cells were measured as a function of distance from the centerpoint in a circular area of 2,927.7 μm^2 (white circle in Fig. S4). This area was selected to include all the signals detected in all cells analyzed. The centerpoint for each cell was manually set as the center of the Golgi defined by the marker GM130. Data series were imported into GraphPad Prism software and the sum of all points were calculated using the Area Under Curve function representing total fluorescence. Data points enclosed in an area of 182.5 μm^2 around the centerpoint (red circle in Fig. S4) were defined as perinuclear with peripheral signal representing the difference between total and perinuclear signal. The boundary of the perinuclear area was set to include most of the Golgi staining for all cells analyzed. All calculations and graphs were performed and generated in Microsoft Excel and GraphPad Prism software. P-values were calculated using unpaired two-tailed Student's *t* test. Figures were prepared in Adobe Photoshop and Illustrator software. Some data for this study were acquired at the Nikon Imaging Center at the Mission Bay campus of UCSF.

Online supplemental material

Fig. S1 shows minimal colocalization between endogenous CHC22 and CHC17, and a modest recruitment of CHC22 to the TGN but not to mitotic spindles in cells depleted of CHC17. Fig. S2 compares CHC22 localization to various cellular markers and includes quantification for data in Fig. 3. Fig. S3 demonstrates that CHC22 distribution is not affected by Brefeldin A treatment. Fig. S4 illustrates the method used for measuring perinuclear vs. peripheral CI-MPR fluorescence. Fig. S5 shows control experiments for STxB uptake assays. Online supplemental material is available at http://www.jcb.org/cgi/content/full/jcb.200908057/DC1.

We thank S. Pfeffer, L. Traub, G. Grosveld, W. Wright, K. Mostov, D. Ganem, and J.M. Bishop for gifts of antibodies, cells, and reagents.

This work was supported by NIH grants GM038093 and DK083589, and a REAC grant from the UCSF School of Medicine to F.M. Brodsky.

Submitted: 11 August 2009
Accepted: 7 December 2009

References

Acton, S.L., D.H. Wong, P. Parham, F.M. Brodsky, and A.P. Jackson. 1993. Alteration of clathrin light chain expression by transfection and gene disruption. *Mol. Biol. Cell.* 4:647–660.

Antonescu, C.N., M. Díaz, G. Femia, J.V. Planas, and A. Klip. 2008. Clathrin-dependent and independent endocytosis of glucose transporter 4 (GLUT4) in myoblasts: regulation by mitochondrial uncoupling. *Traffic.* 9:1173–1190. doi:10.1111/j.1600-0854.2008.00755.x

Arighi, C.N., L.M. Hartnell, R.C. Aguilar, C.R. Haft, and J.S. Bonifacino. 2004. Role of the mammalian retromer in sorting of the cation-independent mannose 6-phosphate receptor. *J. Cell Biol.* 165:123–133. doi:10.1083/jcb.200312055

Banting, G., R. Maile, and E.P. Roquemore. 1998. The steady state distribution of humTGN46 is not significantly altered in cells defective in clathrin-mediated endocytosis. *J. Cell Sci.* 111:3451–3458.

Benmerah, A., and C. Lamaze. 2007. Clathrin-coated pits: vive la différence? *Traffic.* 8:970–982. doi:10.1111/j.1600-0854.2007.00585.x

Bennett, E.M., S.X. Lin, M.C. Towler, F.R. Maxfield, and F.M. Brodsky. 2001. Clathrin hub expression affects early endosome distribution with minimal impact on receptor sorting and recycling. *Mol. Biol. Cell.* 12:2790–2799.

Bolte, S., and F.P. Cordelières. 2006. A guided tour into subcellular colocalization analysis in light microscopy. *J. Microsc.* 224:213–232. doi:10.1111/j.1365-2818.2006.01706.x

Borner, G.H., M. Harbour, S. Hester, K.S. Lilley, and M.S. Robinson. 2006. Comparative proteomics of clathrin-coated vesicles. *J. Cell Biol.* 175:571–578. doi:10.1083/jcb.200607164

Brodsky, F.M. 1985. Clathrin structure characterized with monoclonal antibodies. I. Analysis of multiple antigenic sites. *J. Cell Biol.* 101:2047–2054. doi:10.1083/jcb.101.6.2047

Brodsky, F.M., C.Y. Chen, C. Knuehl, M.C. Towler, and D.E. Wakeham. 2001. Biological basket weaving: formation and function of clathrin-coated vesicles. *Annu. Rev. Cell Dev. Biol.* 17:517–568. doi:10.1146/annurev.cellbio.17.1.517

Brüning, J.C., M.D. Michael, J.N. Winnay, T. Hayashi, D. Hörsch, D. Accili, L.J. Goodyear, and C.R. Kahn. 1998. A muscle-specific insulin receptor knockout exhibits features of the metabolic syndrome of NIDDM without altering glucose tolerance. *Mol. Cell.* 2:559–569. doi:10.1016/S1097-2765(00)80155-0

Bujny, M.V., V. Popoff, L. Johannes, and P.J. Cullen. 2007. The retromer component sorting nexin-1 is required for efficient retrograde transport of Shiga toxin from early endosome to the trans Golgi network. *J. Cell Sci.* 120:2010–2021. doi:10.1242/jcs.003111

Chen, C.Y., and F.M. Brodsky. 2005. Huntingtin-interacting protein 1 (Hip1) and Hip1-related protein (Hip1R) bind the conserved sequence of clathrin light chains and thereby influence clathrin assembly in vitro and actin distribution in vivo. *J. Biol. Chem.* 280:6109–6117. doi:10.1074/jbc.M408454200

Dell'Angelica, E.C., H. Ohno, C.E. Ooi, E. Rabinovich, K.W. Roche, and J.S. Bonifacino. 1997. AP-3: an adaptor-like protein complex with ubiquitous expression. *EMBO J.* 16:917–928. doi:10.1093/emboj/16.5.917

Fazakerley, D.J., S.P. Lawrence, V.A. Lizunov, S.W. Cushman, and G.D. Holman. 2009. A common trafficking route for GLUT4 in cardiomyocytes in response to insulin, contraction and energy-status signalling. *J. Cell Sci.* 122:727–734. doi:10.1242/jcs.041178

Frittoli, E., A. Palamidessi, A. Pizzigoni, L. Lanzetti, M. Garrè, F. Troglio, A. Troilo, M. Fukuda, P.P. Di Fiore, G. Scita, and S. Confalonieri. 2008. The primate-specific protein TBC1D3 is required for optimal macropinocytosis in a novel ARF6-dependent pathway. *Mol. Biol. Cell.* 19:1304–1316. doi:10.1091/mbc.E07-06-0594

Ganley, I.G., E. Espinosa, and S.R. Pfeffer. 2008. A syntaxin 10-SNARE complex distinguishes two distinct transport routes from endosomes to the trans-Golgi in human cells. *J. Cell Biol.* 180:159–172. doi:10.1083/jcb.200707136

Garvey, W.T., L. Maianu, J.H. Zhu, G. Brechtel-Hook, P. Wallace, and A.D. Baron. 1998. Evidence for defects in the trafficking and translocation of GLUT4 glucose transporters in skeletal muscle as a cause of human insulin resistance. *J. Clin. Invest.* 101:2377–2386. doi:10.1172/JCI1557

He, W., M.S. Ladinsky, K.E. Huey-Tubman, G.J. Jensen, J.R. McIntosh, and P.J. Björkman. 2008. FcRn-mediated antibody transport across epithelial cells revealed by electron tomography. *Nature.* 455:542–546. doi:10.1038/nature07255

Hehnly, H., D. Sheff, and M. Stamnes. 2006. Shiga toxin facilitates its retrograde transport by modifying microtubule dynamics. *Mol. Biol. Cell.* 17:4379–4389. doi:10.1091/mbc.E06-04-0310

Hinrichsen, L., J. Harborth, L. Andrees, K. Weber, and E.J. Ungewickell. 2003. Effect of clathrin heavy chain- and alpha-adaptin-specific small inhibitory RNAs on endocytic accessory proteins and receptor trafficking in HeLa cells. *J. Biol. Chem.* 278:45160–45170. doi:10.1074/jbc.M307290200

Hood, F.E., and S.J. Royle. 2009. Functional equivalence of the clathrin heavy chains CHC17 and CHC22 in endocytosis and mitosis. *J. Cell Sci.* 122:2185–2190. doi:10.1242/jcs.046177

Hou, J.C., and J.E. Pessin. 2007. Ins (endocytosis) and outs (exocytosis) of GLUT4 trafficking. *Curr. Opin. Cell Biol.* 19:466–473. doi:10.1016/j.ceb.2007.04.018

Huang, F., A. Khvorova, W. Marshall, and A. Sorkin. 2004. Analysis of clathrin-mediated endocytosis of epidermal growth factor receptor by RNA interference. *J. Biol. Chem.* 279:16657–16661. doi:10.1074/jbc.C400046200

Huang, S., and M.P. Czech. 2007. The GLUT4 glucose transporter. *Cell Metab.* 5:237–252. doi:10.1016/j.cmet.2007.03.006

Johannes, L., and V. Popoff. 2008. Tracing the retrograde route in protein trafficking. *Cell.* 135:1175–1187. doi:10.1016/j.cell.2008.12.009

Karylowski, O., A. Zeigerer, A. Cohen, and T.E. McGraw. 2004. GLUT4 is retained by an intracellular cycle of vesicle formation and fusion with endosomes. *Mol. Biol. Cell.* 15:870–882. doi:10.1091/mbc.E03-07-0517

Kedra, D., M. Peyrard, I. Fransson, J.E. Collins, I. Dunham, B.A. Roe, and J.P. Dumanski. 1996. Characterization of a second human clathrin heavy chain polypeptide gene (CLH-22) from chromosome 22q11. *Hum. Mol. Genet.* 5:625–631. doi:10.1093/hmg/5.5.625

Kerr, M.C., M.R. Lindsay, R. Luetterforst, N. Hamilton, F. Simpson, R.G. Parton, P.A. Gleeson, and R.D. Teasdale. 2006. Visualisation of macropinosome maturation by the recruitment of sorting nexins. *J. Cell Sci.* 119:3967–3980. doi:10.1242/jcs.03167

Li, L.V., and K.V. Kandror. 2005. Golgi-localized, gamma-ear-containing, Arf-binding protein adaptors mediate insulin-responsive trafficking of glucose transporter 4 in 3T3-L1 adipocytes. *Mol. Endocrinol.* 19:2145–2153. doi:10.1210/me.2005-0032

Lim, J.P., J.T. Wang, M.C. Kerr, R.D. Teasdale, and P.A. Gleeson. 2008. A role for SNX5 in the regulation of macropinocytosis. *BMC Cell Biol.* 9:58. doi:10.1186/1471-2121-9-58

Liu, S.-H., M.C. Towler, E. Chen, C.-Y. Chen, W. Song, G. Apodaca, and F.M. Brodsky. 2001. A novel clathrin homolog that co-distributes with cytoskeletal components functions in the trans-Golgi network. *EMBO J.* 20:272–284. doi:10.1093/emboj/20.1.272

Lombardi, D., T. Soldati, M.A. Riederer, Y. Goda, M. Zerial, and S.R. Pfeffer. 1993. Rab9 functions in transport between late endosomes and the trans Golgi network. *EMBO J.* 12:677–682.

Maianu, L., S.R. Keller, and W.T. Garvey. 2001. Adipocytes exhibit abnormal subcellular distribution and translocation of vesicles containing glucose transporter 4 and insulin-regulated aminopeptidase in type 2 diabetes mellitus: implications regarding defects in vesicle trafficking. *J. Clin. Endocrinol. Metab.* 86:5450–5456. doi:10.1210/jc.86.11.5450

Mallard, F., C. Antony, D. Tenza, J. Salamero, B. Goud, and L. Johannes. 1998. Direct pathway from early/recycling endosomes to the Golgi apparatus revealed through the study of shiga toxin B-fragment transport. *J. Cell Biol.* 143:973–990. doi:10.1083/jcb.143.4.973

Mallard, F., B.L. Tang, T. Galli, D. Tenza, A. Saint-Pol, X. Yue, C. Antony, W. Hong, B. Goud, and L. Johannes. 2002. Early/recycling endosomes-to-TGN transport involves two SNARE complexes and a Rab6 isoform. *J. Cell Biol.* 156:653–664. doi:10.1083/jcb.200110081

Mardones, G.A., P.V. Burgos, D.A. Brooks, E. Parkinson-Lawrence, R. Mattera, and J.S. Bonifacino. 2007. The trans-Golgi network accessory protein p56 promotes long-range movement of GGA/clathrin-containing transport carriers and lysosomal enzyme sorting. *Mol. Biol. Cell.* 18:3486–3501. doi:10.1091/mbc.E07-02-0190

Meyer, C., D. Zizioli, S. Lausmann, E.L. Eskelinen, J. Hamann, P. Saftig, K. von Figura, and P. Schu. 2000. mu1A-adaptin-deficient mice: lethality, loss of AP-1 binding and rerouting of mannose 6-phosphate receptors. *EMBO J.* 19:2193–2203. doi:10.1093/emboj/19.10.2193

Michael, M.D., R.N. Kulkarni, C. Postic, S.F. Previs, G.I. Shulman, M.A. Magnuson, and C.R. Kahn. 2000. Loss of insulin signaling in hepatocytes leads to severe insulin resistance and progressive hepatic dysfunction. *Mol. Cell.* 6:87–97. doi:10.1016/S1097-2765(00)00010-1

Motley, A., N.A. Bright, M.N. Seaman, and M.S. Robinson. 2003. Clathrin-mediated endocytosis in AP-2-depleted cells. *J. Cell Biol.* 162:909–918. doi:10.1083/jcb.200305145

Nokes, R.L., I.C. Fields, R.N. Collins, and H. Fölsch. 2008. Rab13 regulates membrane trafficking between TGN and recycling endosomes in polarized epithelial cells. *J. Cell Biol.* 182:845–853. doi:10.1083/jcb.200802176

Popoff, V., G.A. Mardones, D. Tenza, R. Rojas, C. Lamaze, J.S. Bonifacino, G. Raposo, and L. Johannes. 2007. The retromer complex and clathrin define an early endosomal retrograde exit site. *J. Cell Sci.* 120:2022–2031. doi:10.1242/jcs.003020

Riederer, M.A., T. Soldati, A.D. Shapiro, J. Lin, and S.R. Pfeffer. 1994. Lysosome biogenesis requires Rab9 function and receptor recycling from endosomes to the trans-Golgi network. *J. Cell Biol.* 125:573–582. doi:10.1083/jcb.125.3.573

Rojas, R., T. van Vlijmen, G.A. Mardones, Y. Prabhu, A.L. Rojas, S. Mohammed, A.J. Heck, G. Raposo, P. van der Sluijs, and J.S. Bonifacino. 2008. Regulation of retromer recruitment to endosomes by sequential action of Rab5 and Rab7. *J. Cell Biol.* 183:513–526. doi:10.1083/jcb.200804048

Saint-Pol, A., B. Yélamos, M. Amessou, I.G. Mills, M. Dugast, D. Tenza, P. Schu, C. Antony, H.T. McMahon, C. Lamaze, and L. Johannes. 2004. Clathrin adaptor epsinR is required for retrograde sorting on early endosomal membranes. *Dev. Cell.* 6:525–538. doi:10.1016/S1534-5807(04)00100-5

Seaman, M.N. 2004. Cargo-selective endosomal sorting for retrieval to the Golgi requires retromer. *J. Cell Biol.* 165:111–122. doi:10.1083/jcb.200312034

Seaman, M.N., M.E. Harbour, D. Tattersall, E. Read, and N. Bright. 2009. Membrane recruitment of the cargo-selective retromer subcomplex is catalysed by the small GTPase Rab7 and inhibited by the Rab-GAP TBC1D5. *J. Cell Sci.* 122:2371–2382. doi:10.1242/jcs.048686

Shepherd, P.R., and B.B. Kahn. 1999. Glucose transporters and insulin action—implications for insulin resistance and diabetes mellitus. *N. Engl. J. Med.* 341:248–257. doi:10.1056/NEJM199907223410406

Shewan, A.M., E.M. van Dam, S. Martin, T.B. Luen, W. Hong, N.J. Bryant, and D.E. James. 2003. GLUT4 recycles via a trans-Golgi network (TGN) subdomain enriched in Syntaxins 6 and 16 but not TGN38: involvement of an acidic targeting motif. *Mol. Biol. Cell.* 14:973–986. doi:10.1091/mbc.E02-06-0315

Sirotkin, H., B. Morrow, R. DasGupta, R. Goldberg, S.R. Patanjali, G. Shi, L. Cannizzaro, R. Shprintzen, S.M. Weissman, and R. Kucherlapati. 1996. Isolation of a new clathrin heavy chain gene with muscle-specific expression from the region commonly deleted in velo-cardio-facial syndrome. *Hum. Mol. Genet.* 5:617–624. doi:10.1093/hmg/5.5.617

Tang, B.L., D.Y. Low, A.E. Tan, and W. Hong. 1998. Syntaxin 10: a member of the syntaxin family localized to the trans-Golgi network. *Biochem. Biophys. Res. Commun.* 242:345–350. doi:10.1006/bbrc.1997.7966

Towler, M.C., P.A. Gleeson, S. Hoshino, P. Rahkila, V. Manalo, N. Ohkoshi, C. Ordahl, R.G. Parton, and F.M. Brodsky. 2004. Clathrin isoform CHC22, a component of neuromuscular and myotendinous junctions, binds sorting nexin 5 and has increased expression during myogenesis and muscle regeneration. *Mol. Biol. Cell.* 15:3181–3195. doi:10.1091/mbc.E04-03-0249

Ungewickell, E.J., and L. Hinrichsen. 2007. Endocytosis: clathrin-mediated membrane budding. *Curr. Opin. Cell Biol.* 19:417–425. doi:10.1016/j.ceb.2007.05.003

van Steensel, B., E.P. van Binnendijk, C.D. Hornsby, H.T. van der Voort, Z.S. Krozowski, E.R. de Kloet, and R. van Driel. 1996. Partial colocalization of glucocorticoid and mineralocorticoid receptors in discrete compartments in nuclei of rat hippocampus neurons. *J. Cell Sci.* 109:787–792.

Vassilopoulos, S., C. Esk, S. Hoshino, B.H. Funke, C.Y. Chen, A.M. Plocik, W.E. Wright, R. Kucherlapati, and F.M. Brodsky. 2009. A role for the CHC22 clathrin heavy-chain isoform in human glucose metabolism. *Science.* 324:1192–1196. doi:10.1126/science.1171529

Wainszelbaum, M.J., A.J. Charron, C. Kong, D.S. Kirkpatrick, P. Srikanth, M.A. Barbieri, S.P. Gygi, and P.D. Stahl. 2008. The hominoid-specific oncogene TBC1D3 activates Ras and modulates epidermal growth factor receptor signaling and trafficking. *J. Biol. Chem.* 283:13233–13242. doi:10.1074/jbc.M800234200

Wakeham, D.E., L. Abi-Rached, M.C. Towler, J.D. Wilbur, P. Parham, and F.M. Brodsky. 2005. Clathrin heavy and light chain isoforms originated by independent mechanisms of gene duplication during chordate evolution. *Proc. Natl. Acad. Sci. USA.* 102:7209–7214. doi:10.1073/pnas.0502058102

Wassmer, T., N. Attar, M.V. Bujny, J. Oakley, C.J. Traer, and P.J. Cullen. 2007. A loss-of-function screen reveals SNX5 and SNX6 as potential components of the mammalian retromer. *J. Cell Sci.* 120:45–54. doi:10.1242/jcs.03302

Wassmer, T., N. Attar, M. Harterink, J.R. van Weering, C.J. Traer, J. Oakley, B. Goud, D.J. Stephens, P. Verkade, H.C. Korswagen, and P.J. Cullen. 2009. The retromer coat complex coordinates endosomal sorting and dynein-mediated transport, with carrier recognition by the trans-Golgi network. *Dev. Cell.* 17:110–122. doi:10.1016/j.devcel.2009.04.016

Williams, D., and J.E. Pessin. 2008. Mapping of R-SNARE function at distinct intracellular GLUT4 trafficking steps in adipocytes. *J. Cell Biol.* 180:375–387. doi:10.1083/jcb.200709108

Wong, D.H., and F.M. Brodsky. 1992. 100-kD proteins of Golgi- and trans-Golgi network-associated coated vesicles have related but distinct membrane binding properties. *J. Cell Biol.* 117:1171–1179. doi:10.1083/jcb.117.6.1171

Zhu, C.H., V. Mouly, R.N. Cooper, K. Mamchaoui, A. Bigot, J.W. Shay, J.P. Di Santo, G.S. Butler-Browne, and W.E. Wright. 2007. Cellular senescence in human myoblasts is overcome by human telomerase reverse transcriptase and cyclin-dependent kinase 4: consequences in aging muscle and therapeutic strategies for muscular dystrophies. *Aging Cell.* 6:515–523. doi:10.1111/j.1474-9726.2007.00306.x